

MICROSTRUCTURE, THERMO-PHYSICAL, MECHANICAL AND WEAR PROPERTIES OF IN-SITU FORMED BORON CARBIDE – ZIRCONIUM DIBORIDE COMPOSITE

[#]T. S. R. CH. MURTHY*·****, SAIRAM ANKATA**, J. K. SONBER*, K. SAIRAM*·****, KULWANT SINGH*, A. NAGARAJ***, P. SENGUPTA*·****, R. D. BEDSE*, SANJIB MAJUMDAR*·****, VIVEKANAND KAIN*·****

*Materials Group, Bhabha Atomic Research Centre, Mumbai, India

**Dept. of Metallurgical and Materials Engineering, Indian Institute of Technology, Kharagpur, India

***Laser and Plasma Technology Division, Bhabha Atomic Research Centre, Mumbai, India

****Homi Bhabha National Institute, Mumbai, India

[#]E-mail: murthi@barc.gov.in

Submitted July 1, 2017; accepted October 20, 2017

Keywords: Boron Carbide, Microstructure, XRD, Electrical resistivity, Thermal conductivity, Wear resistance

Microstructure, thermos-physical, mechanical and wear properties of in-situ formed B_4C - ZrB_2 composite were investigated. Coefficient of thermal expansion, thermal diffusivity and electrical resistivity of the composite were measured at different temperatures up to $1000^\circ C$ in inert atmosphere. Flexural strength was measured up to $900^\circ C$ in air. Friction and wear properties have been studied at different loads under reciprocative sliding, using a counter body (ball) of cemented tungsten carbide (WC-Co) at ambient conditions. X-ray diffraction (XRD) and electron probe microanalysis (EPMA) confirmed the formation of ZrB_2 as the reaction product in the composite. Electrical resistivity was measured as $3.02 \times 10^{-4} \Omega \cdot m$ at $1000^\circ C$. Thermal conductivity measured at temperatures between $25^\circ C$ and $1000^\circ C$ was in the range of 8 to $10 W \cdot (m \cdot K)^{-1}$. Flexural strength of the composite decreased with increase in temperature and reached a value of $92 MPa$ at $900^\circ C$. The average value of coefficient of friction (COF) was measured as 0.15 at $20 N$ load and $10 Hz$ frequency. Increase of load from $5 N$ to $20 N$ resulted in decrease in COF from 0.24 to 0.15 at $10 Hz$ frequency. Specific wear rate data observed was of the order of $10^{-5} mm^3 \cdot (N \cdot m)^{-1}$. Both abrasive and tribo-chemical reaction wear mechanisms were observed on the worn surface of flat and counter body materials. At higher loads ($\geq 10 N$) a tribo-chemical reaction wear mechanism was dominant.

INTRODUCTION

Boron carbide (B_4C) is a potential material for heavy duty wear applications, cutting tools, armor and neutron absorbers in various types of nuclear reactors (Pressurized water reactor, boiling water reactor, fast breeder reactor and high temperature reactors), due to its high melting point, hardness, wear resistance, moderate electrical and thermal conductivity, chemical stability, retention of strength at elevated temperatures and high neutron absorption cross-section for both thermal and fast neutrons [1-15]. Important properties of boron carbide are listed in Table 1 [3,16]. Despite its combination of attractive properties, the usage of B_4C is limited in real life due to difficulties in densification and susceptibility to brittle failure [3, 17]. Covalent bonding prevalent in B_4C necessitates high sintering temperatures close to the melting point for achieving full dense compacts [3, 18, 19]. Significant improvement in densification was observed when particles of nanometer or submicron size are used for sintering [19]. Alternative methods for obtaining full density with good mechanical/physical properties are summarized below.

Continuous research on boron carbide based ceramics has proven that suitable second phase addition helps

in achieving improved sintering behavior and mechanical properties [3, 19, 20]. Additions of reducing elements such as carbon, silicon and aluminum containing additives such as SiC, Be_2C , TiC, AlN enhance the sintering kinetics by removing the surface oxide layers of boron carbide (usually B_2O_3 layer is present on B_4C particles, which hinders densification) [3, 17, 19]. Metallic additives (such as Fe and Cu) facilitate liquid phase sintering and thus help in achieving dense bodies at lower sintering temperatures [3, 19]. However, metallic additives are detrimental to the unique properties of the hard ceramics [3]. Alternatively, addition of non-metallic sinter additives such as oxides, nitrides, carbides, borides (such as AlN, BN, ZrB_2 , HfB_2) can enhance the densification as well as mechanical/physical properties [3, 17-19]. Advanced sintering techniques like spark plasma sintering or flash sintering also reported that full density can be achieved at lower sintering temperatures in a short span of holding time (10 to 15 minutes) [18, 21].

Oxide additions as sintering aids are particularly interesting due to the chemical instability of B_4C with respect to many oxides [19, 22]. The resulting chemical reactions during sintering not only enhances the densification but also improves the thermo-mechanical and physical properties of dense bodies via the formation

of reaction products such as carbides or borides [3, 19, 22, 23]. The in-situ reaction of B_4C with Me oxides (Me = Ti, Zr, Cr, V, Hf, Eu, La, and Y) yielded high dense B_4C based composites (B_4C -MeB₂ composites) at a lower sintering temperatures with improved mechanical properties compared to monolithic boron carbide [3, 19, 22, 23]. It is reported that TiO_2 addition to B_4C has helped to enhance the densification, due to the formation of sub-stoichiometric B_4C by reactive sintering [19, 24]. This sub-stoichiometric compound is believed to enhance the mobility of the constituents, resulting in higher sinterability [19, 24]. The reaction between HfO_2 and B_4C results in the formation of B_4C -HfB₂ composites with improved thermo-mechanical properties as compared to monolithic B_4C [19]. Sairam et al. [19] reported fully dense B_4C -HfB₂ composites obtained by in-situ reaction of B_4C and 2.5 % HfO_2 during hot pressing at a temperature of 1900°C and a pressure of 40 MPa (under vacuum). Similarly, it is reported that the addition of ZrO_2 is beneficial for densification due to the formation of ZrB_2 as a reaction product [22].

Tribology studies on monolithic boron carbide, B_4C -BN (hexagonal) composites and SiC- B_4C -Si cermets have been reported in the literature [25-27]. The coefficient of friction of boron carbide has been reported as low as 0.03, but some reports recorded values up to 0.9 [25-27], depending on the load, surface chemical composition, counter body material and humidity. During tribological tests, B_4C undergoes oxidation, which results in the formation of B_2O_3 , which further converts to a boric acid (H_3BO_3) film in the presence of sufficient humidity [25, 28-31]. Boric acid based films reduce the friction by forming a smooth friction surface at the interface, acting as lubricants due to their layered structure [28].

There is a demand for wear resistant components, which are used in mechanical systems that involve high temperatures, heavy loads, aggressive environments and high velocities. Refractory metal borides, carbides and their composites are natural candidates for these tribological applications due to their exceptional hardness, elastic modulus and thermal stability at elevated temperatures [32-38]. Among these, boron carbide is one of the potential materials for wear resistant applications

[25]. However, difficulties in consolidation, poor fracture toughness and moderate oxidation resistance restrict the widespread use of B_4C [1, 3]. Preparation of in-situ formed B_4C composites containing ZrB_2 appears as a viable solution to overcome the above limitations [22]. Although in-situ formed B_4C - ZrB_2 composites were reported in literature, the detailed characterization with respect to microstructure, thermophysical, mechanical and wear properties are rather limited. It is believed that the presence of second phases, especially ZrB_2 , will be helpful to enhance the thermo-physical and mechanical properties of boron carbide.

In this study, the microstructure, thermo-physical, mechanical and wear properties of in-situ formed B_4C - ZrB_2 composite are investigated. Microstructural characterization is carried out using a scanning electron microscope (SEM) with energy dispersive spectroscopy (EDS) and wavelength dispersive spectroscopy (WDS), i.e. electron probe microanalysis (EPMA). coefficient of thermal expansion (CTE), thermal diffusivity and electrical resistivity are measured up to 1000°C in an inert atmosphere. Flexural strength is measured up to 900°C in air. Friction and wear properties of this composite have been studied at different loads under reciprocative sliding, using a counter body (ball) of cemented tungsten carbide (WC-Co).

EXPERIMENTAL

Starting materials and consolidation

Boron carbide (B_4C : 78.5 % B, 19.5 % C, < 1 % O, 0.02 % Fe, 0.02 % Si; Vajrabor HP3.5, Bhukhanvala) and reactor grade zirconium oxide, ZrO_2 (impurities: 600 ppm Fe, 300 ppm Ca, 150 ppm Ti, 100 ppm Cr, 100 ppm Hf; RG, Nuclear Fuel Complex) were used to prepare dense B_4C - ZrB_2 composite in the present study. The weighed quantities of 95 wt. % B_4C and 5 wt. % ZrO_2 powders were mixed in a turbo mixer (MXM-2, Insmart Systems) for 4 h. The particle size distribution (Figure 1a) of mixed powders was measured by laser diffraction (PSA 1064L, CILAS). The morphology of mixed powders was examined by SEM (MV2300CT/100, Camscan) and is presented in Figure 1b. X-ray diffraction (XRD) patterns of starting mixed powders were obtained by using a X-ray diffractometer (PW1830, Philips) with Ni-filtered Cu-K α radiation for phase identification as presented in Figure 2a.

The powder mixture was weighed and loaded into a high density multi cavity graphite die with a cavity of 60 mm inner diameter and 50 mm height. The die cavity was coated with hexagonal boron nitride (h-BN, ESK Ceramics) in order to avoid carbon diffusion from the graphite material. Reaction hot pressing was conducted in a high temperature, high vacuum hot press at 1800°C for 1 h with a pressure of 30 MPa under a vacuum of 10^{-5} mbar.

Table 1. Important properties of B_4C [3, 16] and ZrB_2 [16].

Property	Boron carbide (B_4C)	ZrB_2
Crystal structure	Rhombohedral	Hexagonal
Density (g/cc)	2.52	6.1
Melting point (°C)	2450	3245
Hardness (GPa)	28 – 37	22 – 26
Fract. toughness (MPa·m ^{1/2})	3.0 – 3.5	4.0 – 6.0
CTE (K)	5.0×10^{-6}	6.8×10^{-6}
Flexural strength (MPa)	300	300
Elastic modulus (GPa)	450 – 470	300 – 350
Electrical resistivity (Ω -m)	10^{-2}	9.2×10^{-8}

Characterization of microstructure and thermos-physical and mechanical properties

The density of the hot-pressed samples was measured using the water displacement method based on Archimedes principle. The theoretical densities of the samples were calculated based on the rule of mixtures by assuming the complete conversion of ZrO₂ into ZrB₂. Densified 60 mm discs were sectioned into various sizes for different characterizations by using electro discharge machining (ultracut S0, Electronica). The cut samples were hot mounted and polished for obtaining mirror finish using a series of diamond suspensions ranging from 15 μm to 0.1 μm grades (Tegramin 25, Struers). XRD patterns were obtained from the polished surface for dense pellet for phase identification and presented in Figure 2b. Further microstructural characterization was carried out by SEM-EDS and EPMA (SX 100, Cameca) with wavelength dispersive spectroscopy (WDS) on the polished surfaces.

Microhardness was measured on the polished surface at a load of 100 gram and dwell time of 15 s. The indentation fracture toughness (K_{IC} – units MPa·m^{1/2}) data was evaluated by crack length measurement of the crack pattern formed around Vickers indents (using a 2 kg load), adopting the model formulation proposed by Anstis et al. [39],

$$K_{IC} = 0.016(E/H)^{1/2}P/c^{3/2} \quad (1)$$

where *E* is the Young's modulus in GPa, *H* the Vickers's hardness in GPa, *P* the applied indentation load in Newton, and *c* the half crack length in mm. The reported values of hardness and fracture toughness are the averages of five measured values. Flexural strength was measured by 3-point bend test in air at room temperature (RT), 500°C and 900°C as per the ASTM C 1161-02C test procedure. The tests were conducted at a crosshead speed of 0.2 mm·min⁻¹ using a screw driven universal testing machine with a span length of 20 mm. Silicon carbide fixtures were used for high temperature tests.

The coefficient of thermal expansion (CTE) was measured up to 1000°C in inert atmosphere using a dual push rod dilatometer (TD 5000S, McScience). Electrical resistivity from room temperature to 1000°C was measured by using the conventional 4-probe method in inert atmosphere. Rectangular cross sectional (dimensions: 1 × 2 × 12 mm) samples were prepared for conductivity measurement. All sides of the sample were cleaned and polished. Four copper probes were connected to the sample with the help of platinum paste. Two probes were located on the two longitudinal sides, which were connected to the programmable current source. The remaining two probes were connected on the top surface in transverse direction with 1 mm apart and connected to a nanovoltmeter, which recorded the output voltage when 100 mA current was passed through the sample.

Thermal diffusivity was measured using a laser flash thermal diffusivity meter. The thermal diffusivity data was corrected for radiation losses and finite pulse width effects. Thermal conductivity (λ) was calculated using the following formula

$$\lambda = \frac{a}{(\rho C_p)} \quad (2)$$

where *a* is the thermal diffusivity, is the geometrical density and *c_p* is the specific heat capacity. More details on the specific heat capacity measurement can be found elsewhere [22].

Tribology study

Tribology studies of in-situ formed B₄C-ZrB₂ composites were carried out in dry (i.e. unlubricated) condition at room temperature and 45 ± 5 % relative humidity, using a ball-on-flat reciprocative sliding wear machine (TR281, DUCOM). A cemented tungsten carbide (WC-Co) ball (AFBMA Grade-10, diameter: 10 mm) was used as the counter body to carry out the experiment. A schematic representation of a similar test configuration is reported elsewhere [32]. Prior to testing, the surface of the flats (the composite) and tungsten carbide balls were cleaned in acetone. The flat samples were mounted on a stationary sample holder. The reciprocative sliding wear tests were conducted at different normal loads of 5 N, 10 N and 20 N against tungsten carbide balls (WC-Co). The sliding frequency was maintained at 10 Hz. The stroke length was fixed at 1 mm. A total sliding time of 10,000 seconds was maintained during the test, resulting in a total sliding distance of 200 m. Wear test parameters are listed in Table 2. The variation in tangential force was recorded using data acquisition software and the corresponding coefficient of friction was calculated automatically. To ensure the reproducibility of the experimental data, tests were repeated twice under identical conditions.

Table 2. Wear test parameters of dry reciprocative sliding test.

Flat material	B ₄ C-ZrB ₂ composite	
	WC-Co cemented ball (AFBMA grade-10)	
Ball material	Diameter	Hardness
	10 mm	22 GPa
Normal load	5, 10, 20 N	
Reciprocal frequency	10 HZ	
Amplitude	1 mm	
Test duration	10000 sec	
Total sliding distance	200 m	
Environment	dry air, T _{room} = 30°C ± 2°C and RH (45 ± 5 %)	

Wear scar analysis

After undergoing the tribology tests, the worn surfaces of both flat and ball were observed using an inverted optical microscope (DMI5000 M, Leica) for determining the dimensions of wear scars. Average values of all the parameters were obtained. The wear scars obtained after the test were examined by using SEM-EDS to identify and provide more insights into the underlying wear mechanism of the composite. EDS elemental mapping data were obtained for the compositional analysis of the worn surfaces. The volume, surface topography, depth and width of the wear scars were measured using a computer-controlled non contacting 3D optical profiler (CCI MP 3D, Taylor Hobson). Prior to testing, the samples were cleaned with acetone using an ultrasonic cleaner.

From the wear volume (V), a specific wear rate was calculated using Equation 3 [40],

$$\text{Specific wear rate} = \frac{V}{P \times s} \quad (3)$$

where V is the wear volume in mm^3 , P is the load in N, s is the total sliding distance in m, which is equal to the number of cycles displacement \times stroke length \times 2, and the specific wear rate is in $(\text{mm}^3 \cdot (\text{N} \cdot \text{m})^{-1})$.

RESULTS

Starting materials

Figure 1a presents the particle size distribution, which indicates at least tri-modal distribution of particles with modes in the sub-micron ($< 0.6 \mu\text{m}$, $\sim 5\%$), $1 \mu\text{m}$ to $3 \mu\text{m}$ (30%) and $3 \mu\text{m}$ to $60 \mu\text{m}$ (65%) ranges. The median particle diameter (D_{50}) is measured as $6.82 \mu\text{m}$. The morphology of the mixed powders was examined by SEM and is presented in Figure 1b; it indicates irregular shaped particles of sizes varying from $1 \mu\text{m}$ to $20 \mu\text{m}$. Figure 2a present the X-ray diffraction pattern of starting

mixed powder, which indicates the presence of B_4C , ZrO_2 and carbon phases. Free carbon associated with the boron carbide is considered as source of carbon in the present study for reactive sintering [3].

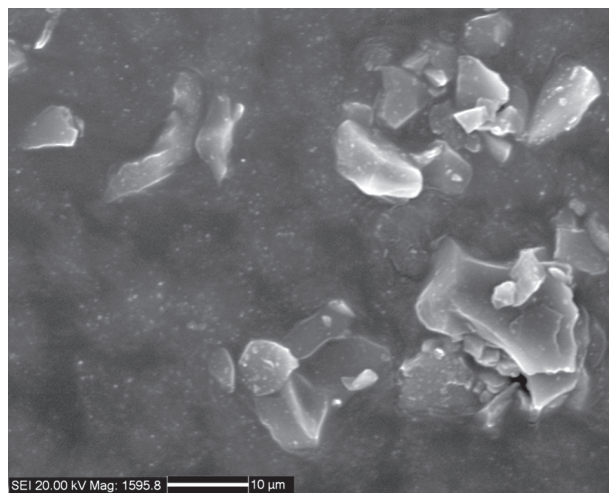
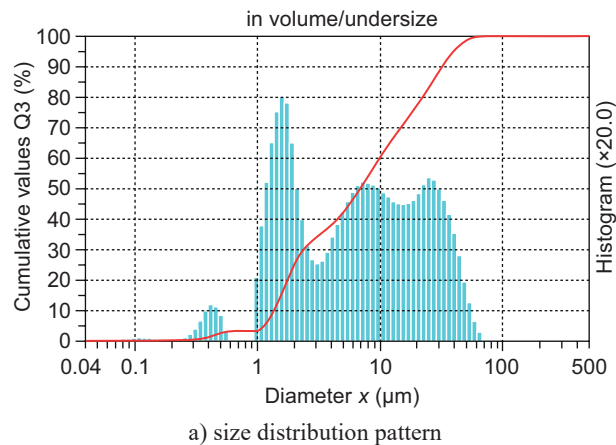


Figure 1. Starting powder particle: a) size distribution pattern and b) morphology of mixed B_4C -5 wt. % ZrO_2 powder.

Table 3. Absolute density, relative density, open porosity, hardness and fracture toughness of B_4C and its composites..

Material	Processing conditions	Absolute density ($\text{g} \cdot \text{cm}^{-3}$)	Relative density (% TD) [#]	Open porosity (%)	Hardness $\text{HV}_{0.1}$ (GPa)	Fracture toughness ($\text{MPa} \cdot \text{m}^{1/2}$)	Reference
B_4C - ZrB_2 (5 wt. % ZrO_2)	1800°C, 1 h, 30 MPa	2.471	95.4	1.4	33 ± 2	3.6 ± 0.5	Present study
* PS B_4C	2275°C, 1 h	2.183	86.6	–	27 ± 3	–	22
* HP B_4C	1900°C, 45 MPa, 3 h	2.394	95.0	–	26 ± 2	3.57	17
* SPS B_4C	1800°C, 50 MPa, 15 min	2.520	100	Nil	37.2	2.8	18
B_4C - HfB_2 (5 wt. % HfO_2)	1900°C, 40 MPa, 1 h	2.606	100	Nil	33 ± 1	4.3 ± 0.4	19
B_4C -30 % MoSi_2	1900°C, 50 MPa, 2 h	2.500	99.2	–	35.1	4.8	20
*PS B_4C - ZrB_2 (5 wt. % ZrO_2)	2275°C, 1 h	2.432	93.9	–	32 ± 1	–	22

* PS – Pressureless sintered, HP – Hot pressed, SPS – Spark plasma sintered; # TD – Theoretical density;

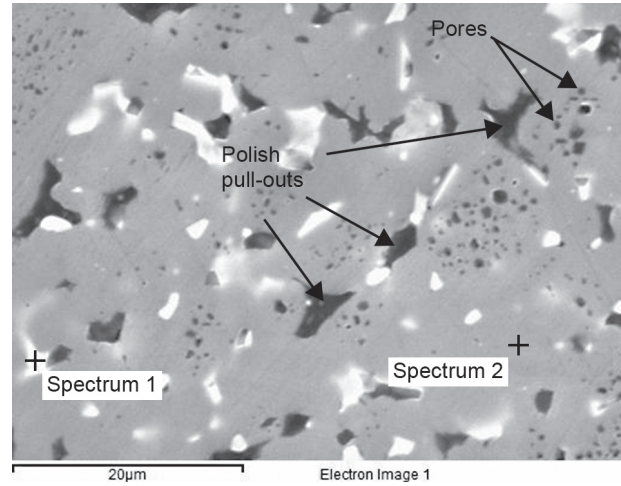
Densification

The hot pressing conditions of in-situ formed B_4C-ZrB_2 composite are presented in Table 3 and compared with the conditions reported earlier [17-20, 22]. The B_4C-ZrB_2 composite is densified to 95.4 % theoretical density (TD) ($2.47 \text{ g}\cdot\text{cm}^{-3}$) under the hot pressing conditions of 1800°C , 1 h, 30 MPa. Open porosity of the composite is measured to be 1.4 %. Similarly, the B_4C-ZrB_2 composite was densified to 93.9 % TD by pressureless sintering at 2275°C with 1 h dwell time [22]. Monolithic boron carbide was densified to 95 % TD and near theoretical density by hot pressing (1900°C and pressure 45 MPa for 3 h) [17] and spark plasma sintering (1800°C and pressure 50 MPa for 15 min) [18] respectively. From the above results and the densification data of Table 3, it is indicated that the addition of ZrO_2 to B_4C is beneficial for obtaining $\geq 95\%$ TD at a relatively lower temperature and pressure.

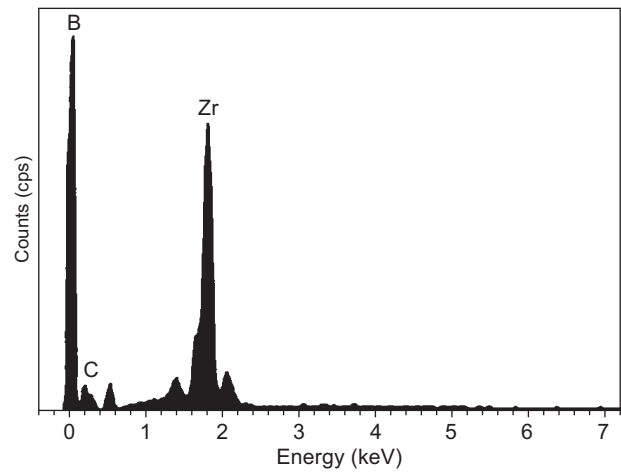
Phase identification and microstructural characterization

The densified (as-sintered) composite was examined by XRD, SEM-EDS and EPMA-WDS for phase identification and elemental distribution in order to understand the reactive sintering mechanism. Figure 2b shows the XRD pattern of composite establishing the phases of B_4C , ZrB_2 and carbon. The absence of ZrO_2 phase in the densified composite indicates that ZrO_2 has reacted with B_4C and/or free carbon and formed ZrB_2 . In order to confirm the presence of reaction products further, these composite was examined by electron microscopy. Figure 3a presents the backscattered electron image of the polished composite, which shows mainly three different phases, namely:

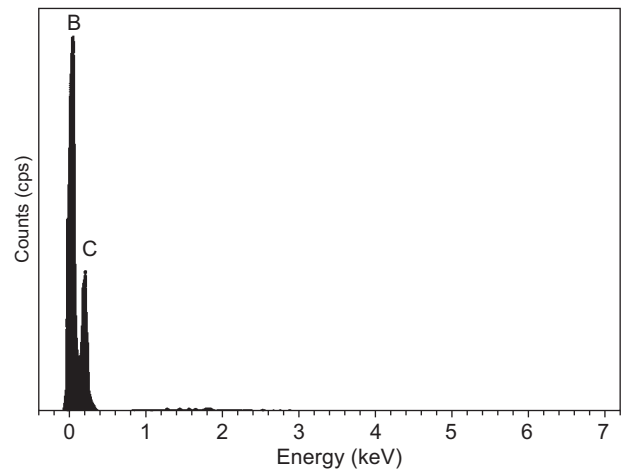
- 1) White phase distributed in matrix,
- 2) Grey phase of matrix and
- 3) Black spots (polish pull outs and/or porosity).



a) back scattered image



b) spectrum-1



c) spectrum-2

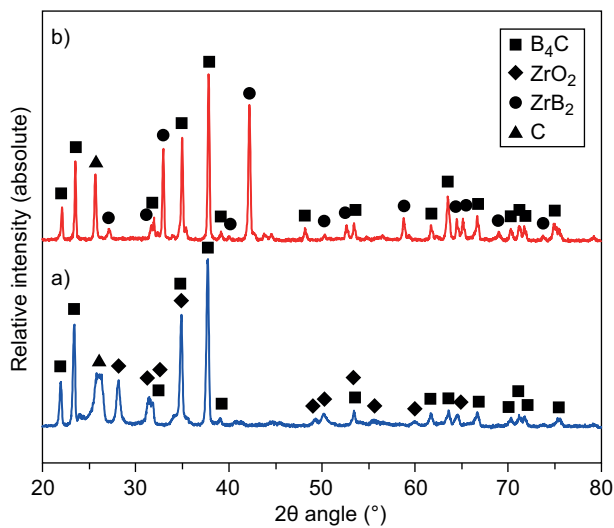
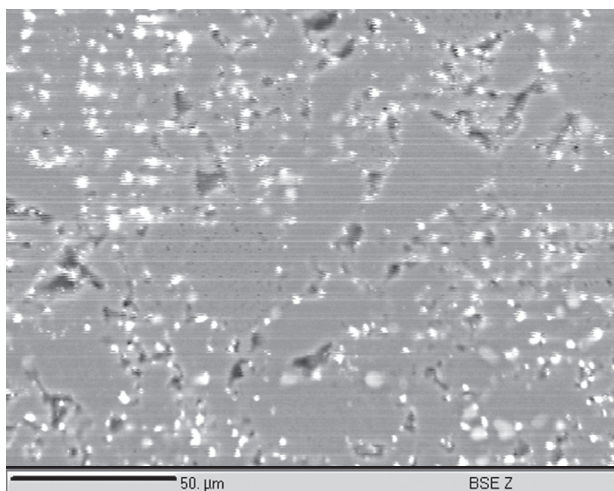


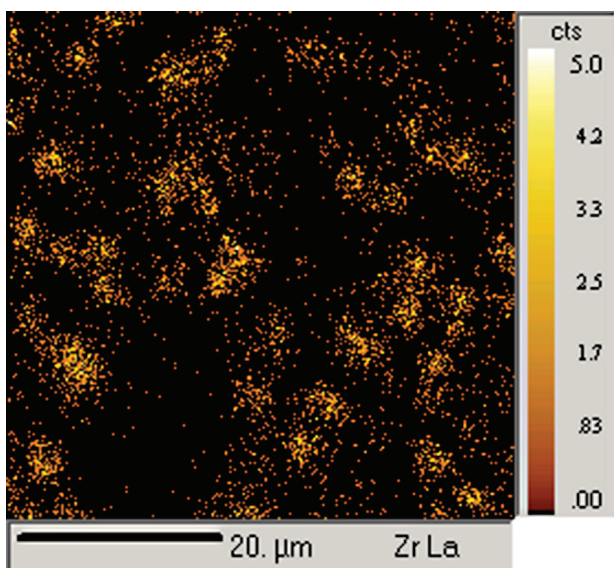
Figure 2. XRD patterns of: a) starting mixed powders of $B_4C-5 \text{ wt. \% } ZrO_2$ and b) in-situ formed B_4C-ZrB_2 composite.

Figure 3. SEM-EDS of in-situ formed B_4C-ZrB_2 composite: a) back scattered image, b) spectrum-1 (white phase – ZrB_2), c) spectrum-2 (matrix – B_4C).

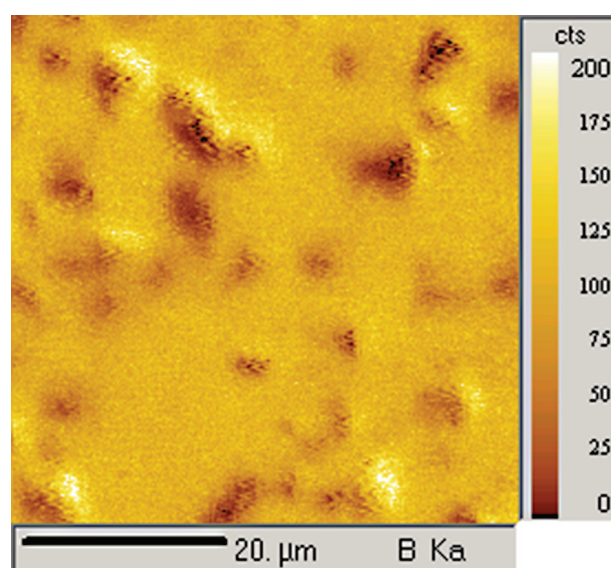


a) back scattered electron image

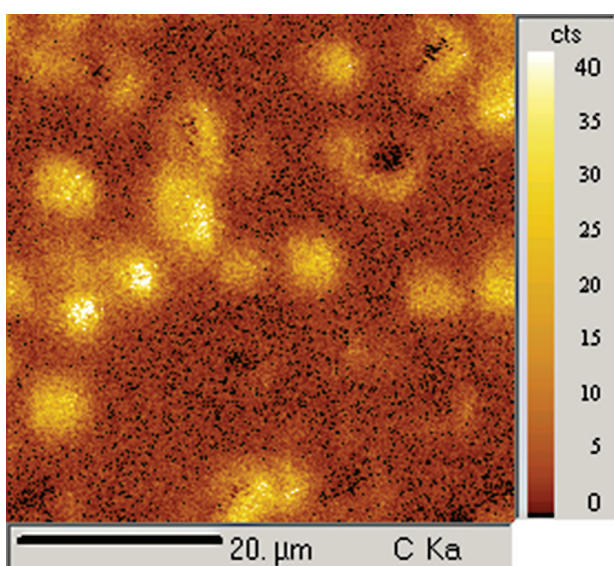
Spot analyses of both white and grey phases were carried out and are presented in Figure 3c and 3d. The white phase was analyzed to contain Zr and B (Spectrum-1) and the gray phase was analyzed to contain B and C (Spectrum-2). The white phase (ZrB_2) is in the size range of 2 - 5 μm and uniformly distributed throughout the matrix. No traces of oxygen are found in the two spectra. Black spots indicate either porosity or polish pull outs. Figure 4 presents the EPMA data on elemental distribution pattern of Zr, C and B, as well as an overlay of all these elements. Based on the elemental mapping results by EDS and EPMA, it could be summarized that the distributed white phase in grey matrix was identified to be ZrB_2 in B_4C matrix.



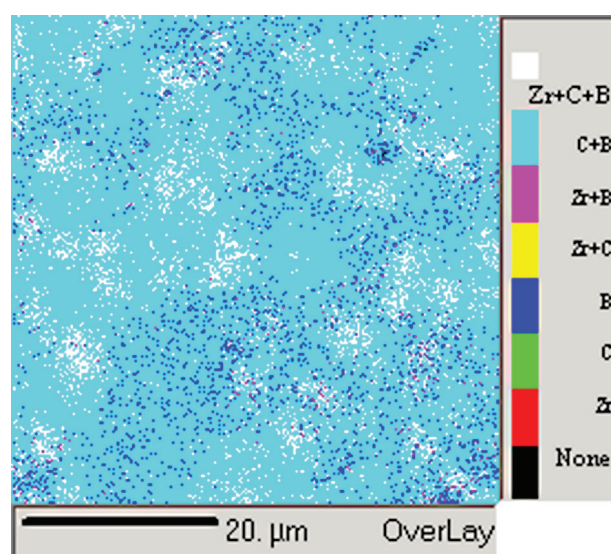
b) Zr



d) B



c) C



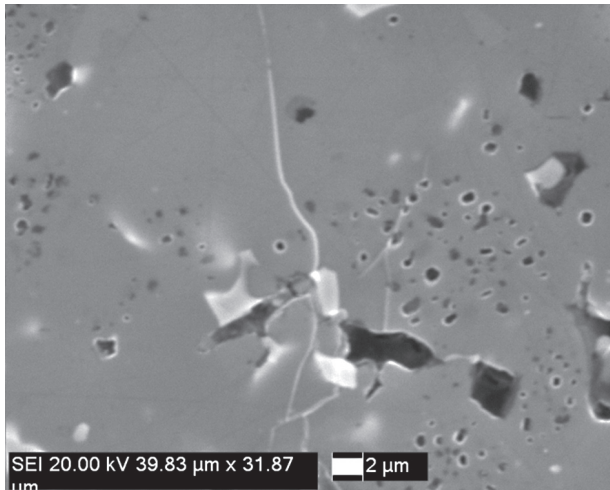
e) overlay of all elements

Figure 4. Electron Probe Micro Analysis (EPMA) of in-situ formed B_4C-ZrB_2 composite: a) back scattered electron image, b) Zr, c) C, d) B, e) overlay of all elements.

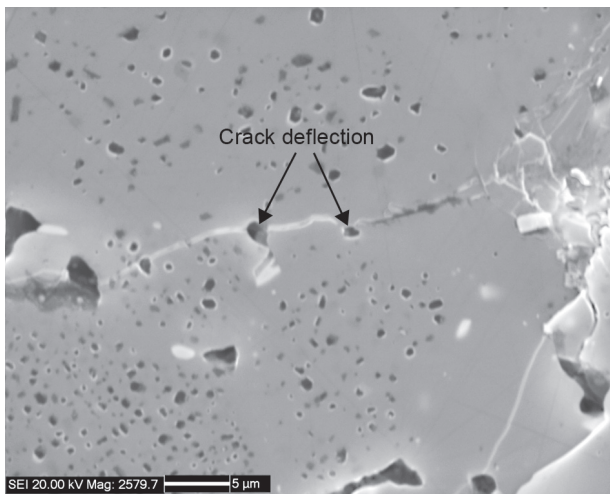
Thermo-physical and mechanical properties

Hardness and indentation fracture toughness values of in-situ formed B_4C-ZrB_2 composite are presented in Table 3. The hardness value of composite is measured as 33 GPa and is comparable with the literature reported values of 26 GPa to 37 GPa for monolithic B_4C and its composites [17-20, 22]. The fracture toughness value of the composite is measured to be $3.6 \text{ MPa}\cdot\text{m}^{1/2}$, which is marginally higher than that for the monolithic boron carbide. Figure 5 presents the crack propagation pattern of in-situ formed B_4C-ZrB_2 composite. Crack arrest and crack deflections as the dominant toughening mechanisms at the pores and second phase regions are observed in Figure 5a and b.

Flexural strength of the composite was measured at room temperature, 500°C and 900°C ; the data are presented in Figure 6. At room temperature, the average



a) crack arrest mechanism



b) crack deflection mechanism

Figure 5. Crack propagation pattern of in-situ formed B_4C-ZrB_2 composite: a) crack arrest mechanism, b) crack deflection mechanism.

flexural strength was measured as 176 GPa. At 500°C the average flexural strength value is 123 GPa, and on further heating to 900°C , the value is reduced 92 GPa. With increasing temperature, a reduction in strength was noticed which could be due to the oxidation of the sample, as the test was conducted in air. The fracture surface of the sample was analyzed to contain an oxidized layer (Figure 7a-d).

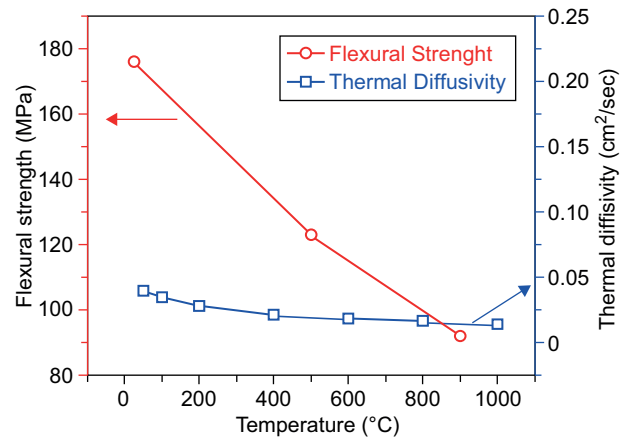


Figure 6. Flexural strength and thermal diffusivity of B_4C-ZrB_2 composite evaluated in inert atmosphere (line joining points are for visual aid only).

Figure 6 presents the thermal diffusivity vs. temperature plot and Table 4 presents the thermal conductivity values at different temperatures. It is observed that the thermal diffusivity decreases with increasing temperature, and a similar trend was noticed in thermal conductivity. The room temperature thermal diffusivity was measured to be $0.0395 \text{ cm}^2\cdot\text{s}^{-1}$ which was decreased to $0.0212 \text{ cm}^2\cdot\text{s}^{-1}$ at 400°C . At high temperature of 1000°C , thermal diffusivity and conductivity are measured as $0.014 \text{ cm}^2\cdot\text{s}^{-1}$ and $7.87 \text{ W}\cdot(\text{m}\cdot\text{K})^{-1}$, respectively. The observed thermal diffusivity/conductivity values of the present studied composite are slightly lower than those of monolithic boron carbide [17]. This could be due to the presence of porosity and the pore shape [41] in the composite of the present study.

Table 4. Thermal diffusivity and conductivity of B_4C-ZrB_2 composite evaluated in inert atmosphere.

Temperature (°C)	Thermal diffusivity (cm ² ·s ⁻¹)	Thermal conductivity (W·m ⁻¹ ·K ⁻¹)
400	0.0212	8.89
600	0.0183	8.64
800	0.0165	8.56
1000	0.014	7.87

Figure 8 presents the electrical resistivity and coefficient of thermal expansion (CTE) plots of B_4C-ZrB_2 composite, which was measured in inert atmosphere up to 1000°C . The value of resistivity is measured as

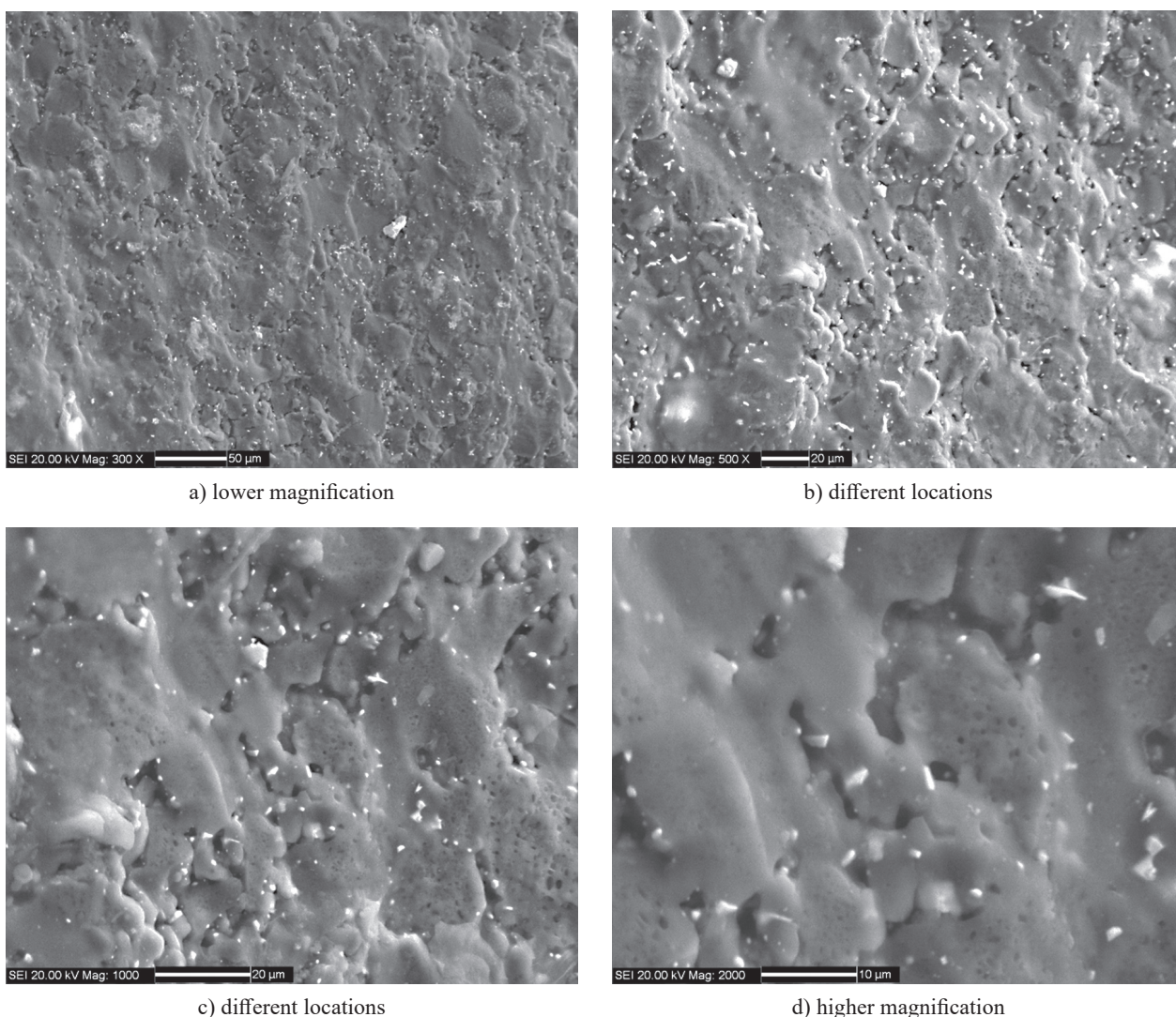


Figure 7. Fractured surface of 3-point bend tested sample (at 900°C) indicates the presence of oxide layer at different locations and magnifications: a) lower magnification, b) and c) at different locations, d) at higher magnification. (white particles are ZrB_2).

$7.27 \times 10^{-4} \Omega\cdot m$, $4.31 \times 10^{-4} \Omega\cdot m$ and $3.02 \times 10^{-4} \Omega\cdot m$ at room temperature (RT), 500°C and 1000°C respectively. A decrease in electrical resistivity was observed with increasing temperature. Sonber et al. [17] reported the higher electrical resistivity of $6.15 \times 10^{-4} \Omega\cdot m$ at 1000°C for monolithic boron carbide. Presence of second phase of ZrB_2 could be the reason for lower electrical resistivity value in the B_4C - ZrB_2 composite. The electrical resistivity of ZrB_2 ($9.2 \times 10^{-8} \Omega\cdot m$) is 6 orders lower than that of B_4C ($\sim 10^{-2} \Omega\cdot m$) [16].

Variation of the CTE with increasing temperature up to 1000°C is plotted in Figure 8. The CTE of B_4C - ZrB_2 composite was measured as $5.01 \times 10^{-6} K^{-1}$ in the temperature range from RT to 1000°C. Literature CTE values of monolithic B_4C and ZrB_2 are $5.0 \times 10^{-6} K^{-1}$ and $6.8 \times 10^{-6} K^{-1}$, respectively in the temperature range from RT to 1000°C [16].

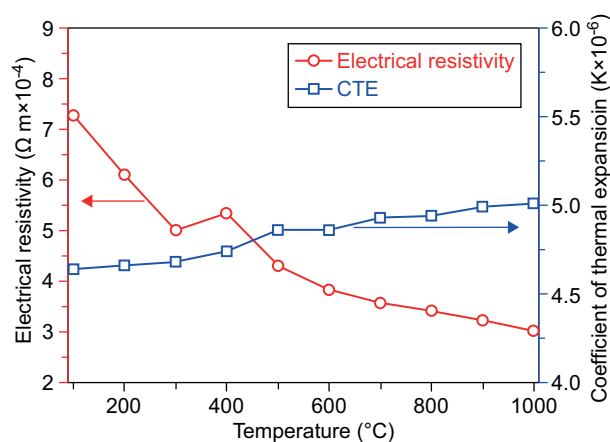


Figure 8. Electrical resistivity and coefficient of thermal expansion of B_4C - ZrB_2 composite evaluated in inert atmosphere (line joining points are for visual aid only).

Coefficient of friction (COF)

To illustrate the frictional response of B₄C–ZrB₂ composite, the variation of the coefficient of friction (COF) with sliding duration for different loads at 10 Hz sliding frequency is presented in Figure 9. The COF is varied within a small range during the entire test period, indicating a stable friction regime. Severity of fluctuation (dynamic COF) is observed to be more predominant at low load (5 N) compared to that at high load (20 N) at 10 Hz frequency. The fluctuations of the friction coefficient during sliding are related to the surface state of tribo-contact regions. Such characteristic features can be attributed to the presence of a third body (wear debris) under sliding motion. Minimal fluctuations were observed at a higher normal load of 20 N. From the above observations, it was found that the COF is a strong function of load, when sliding against cemented WC–Co. An average dynamic COF was calculated at all the loads and is presented in Table 5 and compared with

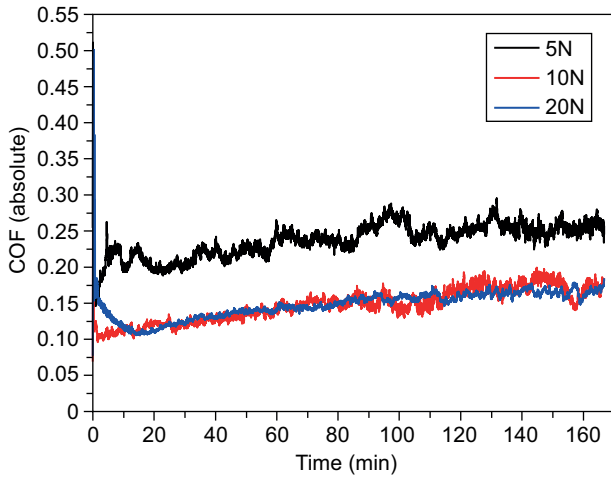


Figure 9. Coefficient of friction (COF) of B₄C-5 wt. % ZrB₂ with a sliding time for different loads at 10 Hz frequency.

values reported in the literature [25, 26]. The dynamic COF values are measured as 0.24 at 5 N load and 0.15 at 10 and 20 N loads. It can be seen that the COF decreases with increasing the load from 5 N to 20 N, i.e. increasing the load from 5 N to 20 N results in a decrease in COF by 37.5 % at 10 Hz frequency. The effect of the normal load on friction response is summarized in Figure 10. COF data of monolithic boron carbide were reported to be 0.15 [25] and 0.59 [26] at 10 N load. The COF of B₄C-5 wt. % h-BN composite was reported as 0.61 [26].

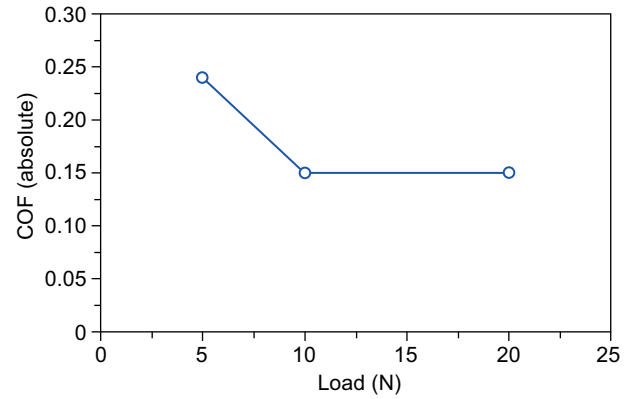


Figure 10. Variation of the COF with applied load at 10 Hz frequency for B₄C–ZrB₂ composite.

Wear scar characteristics

The surface profiles of wear scars were studied to determine the depth and width of the wear scars orthogonal to the sliding direction using a 3D optical profilometer and optical microscope. Optical micrographs of the wear scars of both the flat and the ball are shown in Figure 11 and Figure 12 respectively. The measured depth and width of wear scars for the flat and ball are summarized in Table 5. The depth profiles of wear scars obtained at 10 Hz frequency for different loads are presented in Figure 13. The depth and

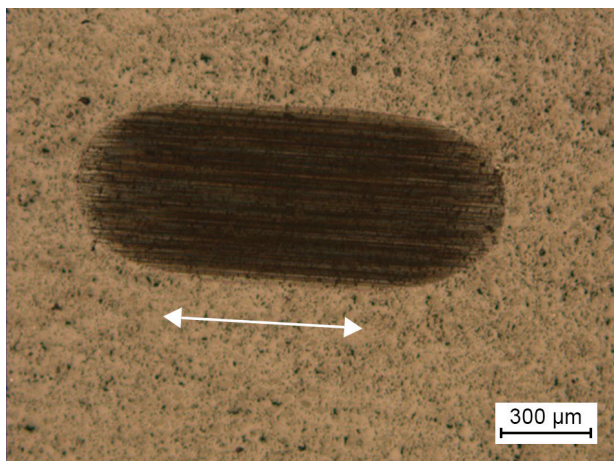
Table 5. Friction and wear data obtained by reciprocative sliding test and 3D-profilometry; all measurements have approximately ± 5 % scatter in values.

Material	Load (N)	Frequency (Hz) or sliding speed (m·s ⁻¹)	Average dynamic COF	Avg flat wear width (mm)	Flat wear depth (µm)	3D wear volume for scar (10 ⁻⁴ mm ³)	Sp. wear rate for scar (10 ⁻⁶ mm ³ ·(N·m) ⁻¹)	Ball wear Dia (mm)	Ball wear volume (10 ⁻⁴ mm ³)	Reference
B ₄ C–ZrB ₂ vs. WC	5	10 Hz	0.24	0.592	2.71	19.42	25.50	0.568	17.11	Present study
	10	10 Hz	0.15	0.728	5.28	44.17	29.01	0.631	25.84	
	20	10 Hz	0.15	0.920	9.73	116.17	38.14	0.836	80.07	
B ₄ C vs. WC	5	10 Hz	0.20	0.523	–	–	3.04	–	–	25
	10	10 Hz	0.15	0.618	–	–	4.26	–	–	
B ₄ C [#] vs. B ₄ C	10	0.656 m s ⁻¹	0.59	–	–	–	~ 210	–	–	26
[#] B ₄ C-5 wt. % hBN vs. B ₄ C	10	0.656 m s ⁻¹	0.61	–	–	–	~ 180	–	–	

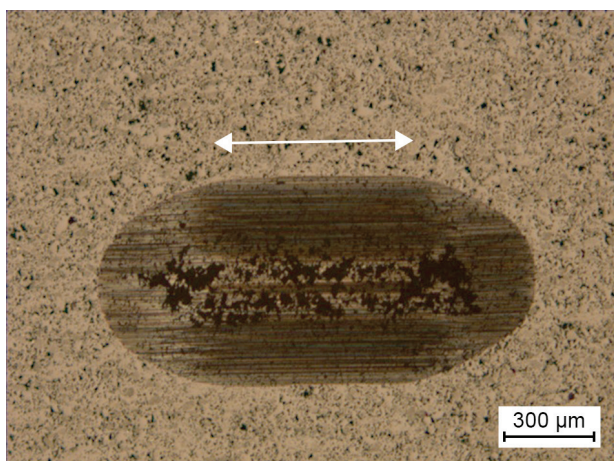
[#] Pin-disc tribometer (Rotation)

width of wear scars are measured to be in the range of 2.71 μm to 9.73 μm and 592 μm to 920 μm , respectively. The scar width from the WC ball (counter body) is found to increase with load and varies from 568 μm to 836 μm (Figure 12). The 3D topographic image of wear scar of

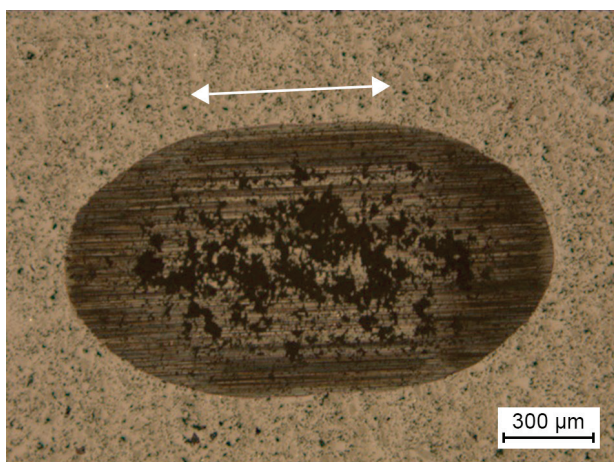
the flat part is presented in Figure 13. Abrasive grooves which are progressively increasing towards the center were observed in flat (B_4C -5 wt. % ZrB_2 composite). Similar abrasive grooves were also identified in the counter body (WC ball), see Figure 12. The width of the



a) 5 N

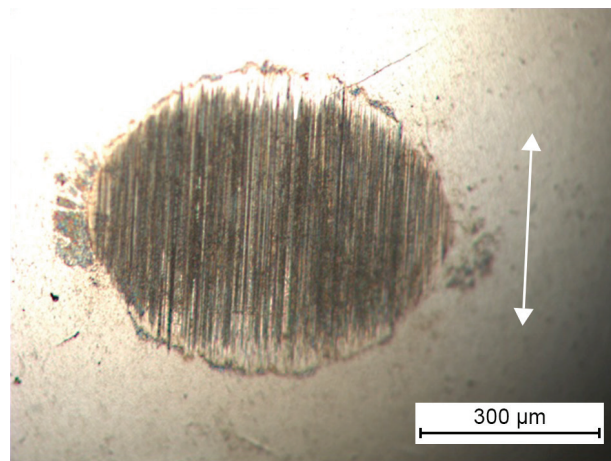


b) 10 N

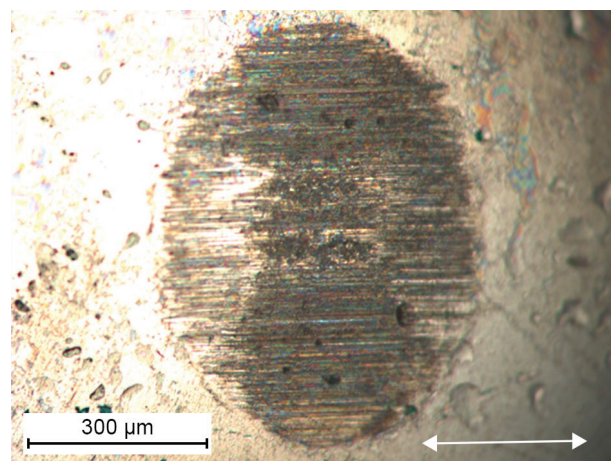


c) 20 N

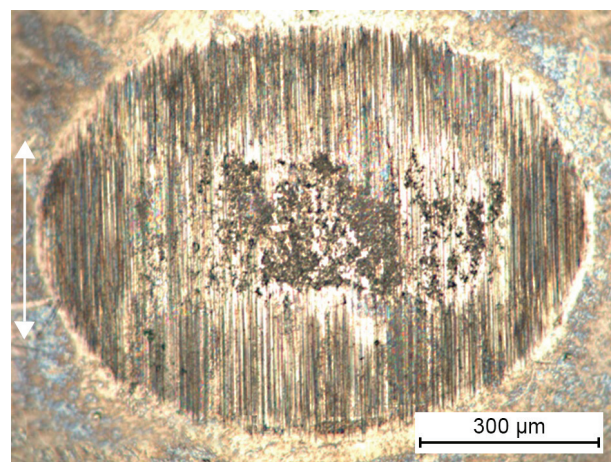
Figure 11. Optical micrograph of the wear scar of B_4C -5 wt. % ZrB_2 at 5 N (a), 10 N (b) and 20 N (c) at 10 Hz frequency. (arrow mark indicates the sliding direction)



a) 5 N



b) 10 N



c) 20 N

Figure 12. Optical micrograph of the wear scar on WC ball at 5 N (a), 10 N (b) and 20 N at 10 Hz frequency. (arrow mark indicates the sliding direction)

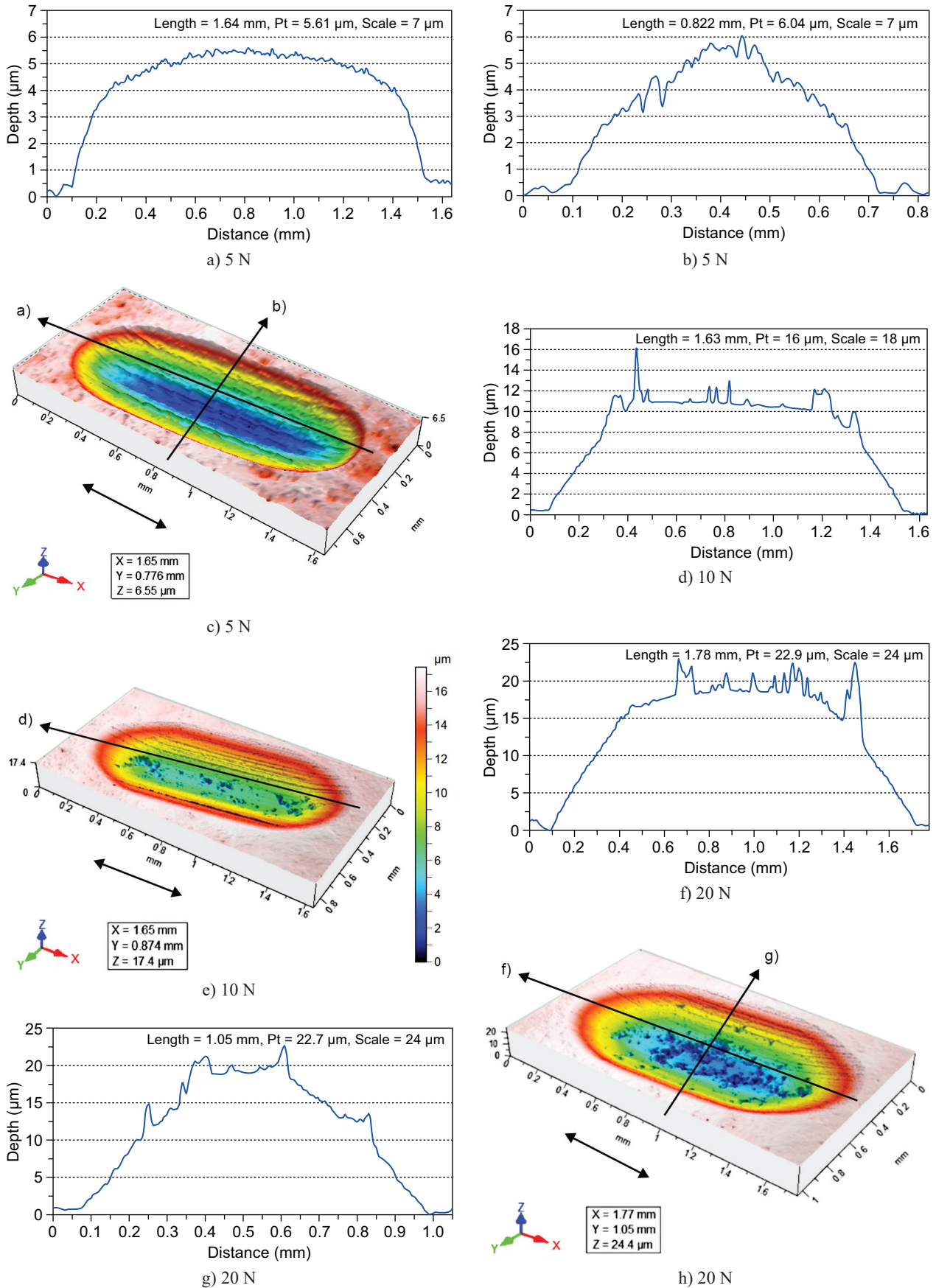


Figure 13. Surface profile and 3D topography of the wear scars of B_4C -5 wt. % ZrB_2 composite, sliding against WC ball at 10 Hz frequency (a, b, c) 5 N, (d, e) 10 N, (f, g, h) 20 N loads. (arrow mark indicates the sliding direction)

wear scar is increased when the load is increased from 5 N to 20 N. It can be inferred that the severity of damage during reciprocative sliding is increased with increasing load. From these findings, it is demonstrated that during sliding wear test, mechanical wear is responsible for formation of abrasive grooves and pullout of material in the flat scar at 5 N load. The intensity of grooves on the wear track is diminished as the load increases due to the formation of a tribo-oxidative chemical layer (Figure 11c and Figure 12c).

The variations of the wear volume and specific wear rate of the B₄C-5 wt. % ZrB₂ composite and the counter body (WC balls) with different loads are presented in Table 5. It can be observed that for a given sliding frequency, the total wear volume of the flat increased with increasing the load. The total wear volume of the flat is increased from $19.42 \times 10^{-4} \text{ mm}^3$ to $116.17 \times 10^{-4} \text{ mm}^3$ with increasing load from 5 N to 20 N at 10 Hz sliding frequency. The highest wear volume of $116.17 \times 10^{-4} \text{ mm}^3$ is observed for bulk B₄C-5 wt. % ZrB₂ tested at 20 N and 10 Hz operating conditions. A similar trend was observed in the specific wear rate also for the flat (Table 5). The specific wear rate has increased from

$25.50 \times 10^{-6} \text{ mm}^3 \cdot (\text{N} \cdot \text{m})^{-1}$ to $38.14 \times 10^{-6} \text{ mm}^3 \cdot (\text{N} \cdot \text{m})^{-1}$ with increasing the load from 5 N to 20 N at 10 Hz frequency. Under similar conditions, the lower specific wear rate of monolithic B₄C was measured as $3.04 \times 10^{-6} \text{ mm}^3 \cdot (\text{N} \cdot \text{m})^{-1}$ and $4.26 \times 10^{-6} \text{ mm}^3 \cdot (\text{N} \cdot \text{m})^{-1}$ respectively for 5 N and 10 N load, respectively [25]. The specific wear rate of monolithic B₄C and B₄C-h-BN composite ($\sim 10^{-4} \text{ mm}^3 \cdot (\text{N} \cdot \text{m})^{-1}$) was reported one order higher than that of the composite in the present study ($\sim 10^{-5} \text{ mm}^3 \cdot (\text{N} \cdot \text{m})^{-1}$) by pin on disc tribo test [26].

As in the case of the counter body (WC ball), the wear volume also increased with increasing load at a constant sliding frequency. The wear volume of the counter body is increased from $17.11 \times 10^{-4} \text{ mm}^3$ to $80.07 \times 10^{-4} \text{ mm}^3$ with an increase of the normal load from 5 N to 20 N at 10 Hz sliding frequency. These results indicate that the overall wear volume of the ball is less compared to that of the flat at all the loads.

Wear scar analysis

SEM images in Figure 14 show the wear scar of the flat under dry conditions. At 5 N load and 10 Hz

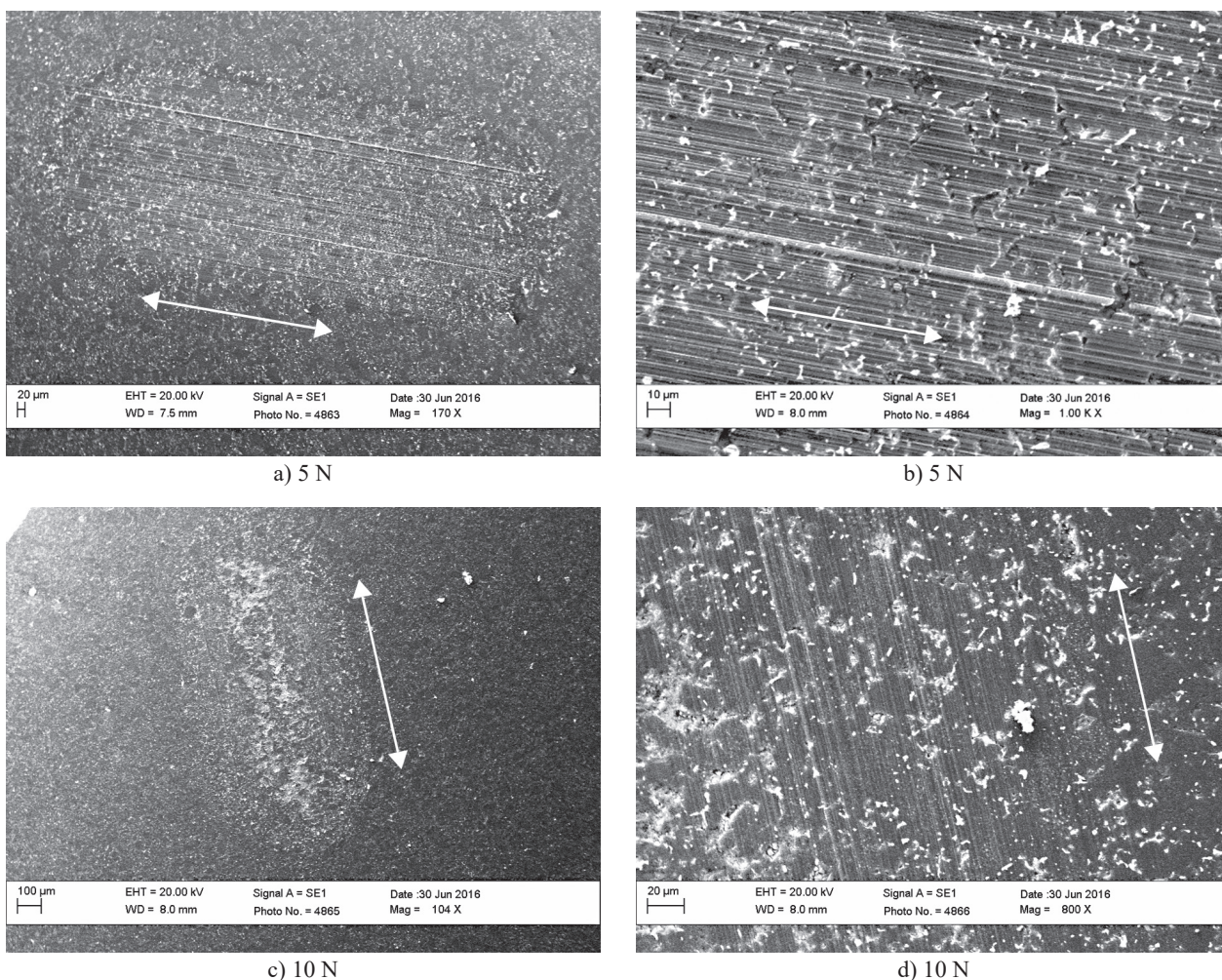


Figure 14. SEM micrographs of wear tracks of flat under dry sliding condition: a), b) 5 N, c), d) 10 N loads at 10 Hz frequency (continue on next page).

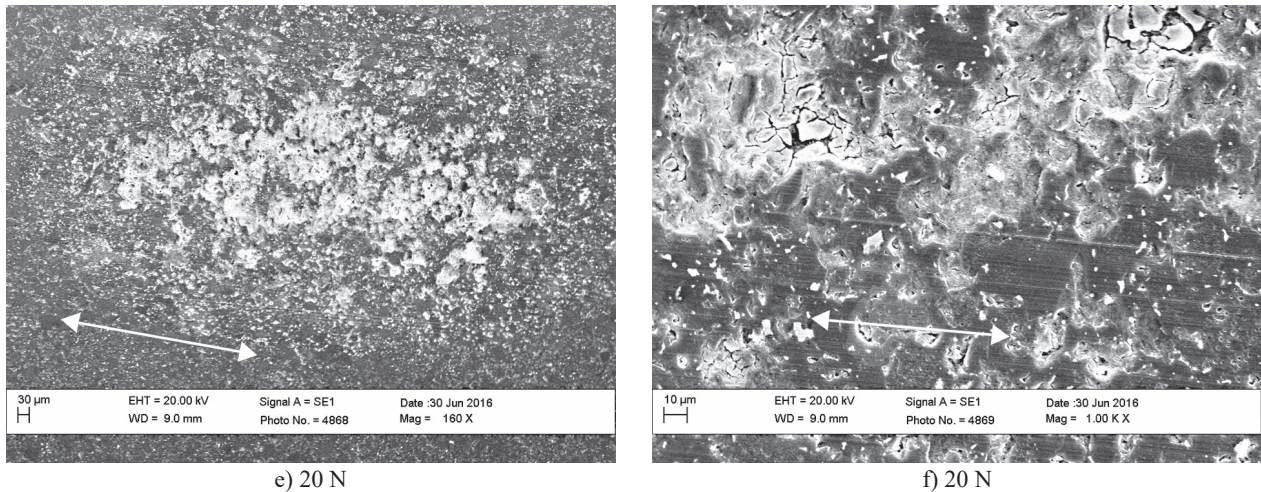


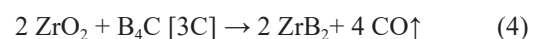
Figure 14. SEM micrographs of wear tracks of flat under dry sliding condition: e), f) 20 N loads at 10 Hz frequency. (arrow mark indicates the sliding direction)

frequency, they show the presence of severe abrasive grooves parallel to the sliding direction with pullouts. At 10 N loads and 10 Hz frequency, mild abrasive grooves along with oxidation were observed in SEM images (Figure 14c and d). Furthermore, EDS analysis confirmed that the dark area on the worn surface of the composite contained a considerable amount of oxygen (due to mild oxidation as shown in Figure 15). In addition to pullout, mild abrasive grooves and tribo-oxidative layer with appreciable fracture on the flat worn surface was observed at higher loads of 20 N. EDS analysis of delaminated layered structure confirmed the presence of O, C, W, Zr and Co, as shown in Figure 15. The intensity of the oxygen signal increases as the load is increased, as evident by the predominant presence of pullout, microcracks and microfracture on the tribolayer, which in accord with the COF data, diminished with load (Figures 9 and 10). Therefore, oxidation plays a crucial role during sliding test at higher loads. Broadly, abrasive grooves, pullouts and microcracks are the most observed characteristic features of wear scar at lower loads. From the data it is evident that the oxidative layer is responsible for a reduced COF at higher loads.

DISCUSSION

Boron carbide possesses strong bonding, low plasticity, high resistance to grain boundary sliding and low surface tension in the solid state. All these factors make densification of powders by sintering difficult [3, 17-19], in spite of having these attractive properties for various engineering applications. In addition, the presence of B_2O_3 on the B_4C surface slows down the densification process. In order to overcome these difficulties, extensive research work was explored throughout world by various methodologies. Recently, advanced sintering techniques like spark plasma and flash sintering have proven useful to obtain near full density compacts. However, these techniques are not exploited commercially on a large scale due to associated setbacks like process cost and sample size. On the other hand, using a suitable sinter additive like in conventional liquid phase sintering by using metallic additives has also been used to reduce the sintering temperature significantly. The presence of metallic additives as a reinforcement phase limits the high temperature applications of sintered compacts. In continuation of works related with sinter additives, it was found that the addition of transition/refractory metal oxides to boron carbide yields B_4C -boride composites by in-situ reaction. This reactive sintering has been reported to enhance the sintering kinetics; as a result, it lowers the effective densification temperature. Goldstein et al. [23] proved the formation of B_4C - metal boride (TiB_2 , ZrB_2 , VB_2 , VB , CrB_2 , YB_2 , YB_4 , LaB_6 , $LaB_6 - ZrB_2$) composites (> 95 % TD) by in situ reaction of B_4C and metal oxide (TiO_2 , ZrO_2 , V_2O_5 , Y_2O_3 , La_2O_3 , $L_2O_3 - ZrO_2$) mixtures [3, 23].

In the present study, the obtained B_4C - ZrB_2 composite formed by in-situ reaction of B_4C - ZrO_2 as per reaction 4.



Carbon for the above reaction is consumed from the

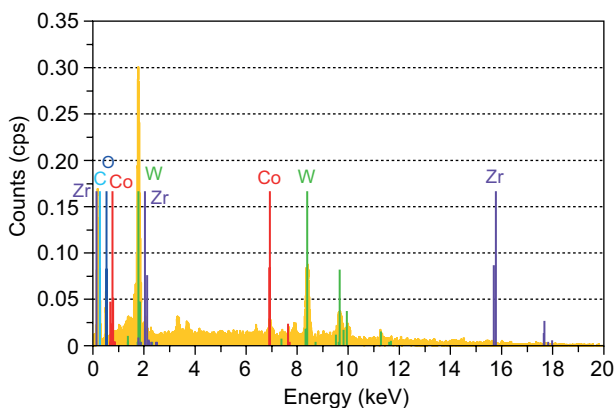


Figure 15. EDS of the wear debris shown on the Figure 14f.

free carbon of boron carbide. No extra carbon was added to the charge. The amount of carbon required for the above reaction for the amount of 5 wt. % ZrO₂ is only 0.73 wt. %. The sample used in our studies was commercially available material produced by carbothermic reduction of boric acid in an Acheson furnace. XRD of the starting boron carbide sample shows the presence of free carbon (Figure 2a). Since B₄C is in equilibrium with free carbon [42] and is the only boundary between B_nC and B_nC-C (where 4 < n < 10) [43], the synthesis of B₄C without free carbon is difficult. The presence of free carbon affects the physical properties of boron carbide [3].

In the present study, > 95 % TD achieved at a hot pressing temperature of 1800°C, 30 MPa, 1 h for B₄C-based composites, whereas for monolithic B₄C, it requires 1900°C, 45 MPa, 3 h [17] for getting the similar density by hot pressing method. XRD (Figure 2b), SEM-EDS (Figure 3) and EPMA-WDS (Figure 4) analysis confirmed the presence of the reaction product ZrB₂ as per reaction 4. From this one can infer that reactive sintering is responsible for lowering the densification temperature, pressure and time. Figure 3 and 5 clearly show the presence of sub-micron sized round pores, in addition to polish pull-outs. The origin of these pores is from one of the gaseous reaction products (CO) as per Equation 4. The presence of sub-micron sized round pores is not harmful, as their size is much below the critical crack length and not having any sharp corners/stress raisers. These pores help to arrest/deflect the cracks (Figures 5a, b) by absorbing energy. In ceramics, failure occurs by the rapid propagation of cracks, resulting in catastrophic failure. Thus increasing the crack propagation resistance by means of crack arrest, crack bridging and crack deflection is crucial for improving the fracture toughness of ceramics and its composites (Figures 5a, b). In the present study, a slight improvement in the fracture toughness was observed due to these mechanisms.

An additional benefit that can be realized by the presence of pores in nuclear applications, is that pores can comfortably accommodate the helium that is generated as a result of neutron irradiation of boron. However, in the composite of the present study, drastic decrease in flexural strength was observed with increasing the temperature to 900°C. This could be due to the oxidation of sample at the test temperature, as the test was carried in air. Non-oxide ceramics are more prone to oxidation at higher temperatures (~ 900°C) in the presence of air as is evident from Figure 7. The morphology of oxidized surfaces clearly indicated the existence of B₂O₃ in molten form (the melting point of B₂O₃ is 450°C).

In a nutshell, consolidation of boron carbide by reactive sintering has many advantages as mentioned below:

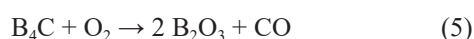
- it lowers the sintering temperature (~ 100°C) compared to monolithic B₄C (Table 3);
- it consumes the free carbon from the boron carbide

(the presence of free carbon deteriorates the properties of boron carbide) [3];

- the presence of sub-micron sized pores helps to crack deflection and arrest mechanisms (improves the fracture toughness);
- the presence of pores also helps to retain the generated helium for control rod applications in nuclear industry and
- the thermophysical and mechanical properties of the composite are improved in comparison to the monolithic boron carbide of similar density (Figures 6 and 8).

Based on the wear data and microscopic analysis of the wear scar, the tribological behavior of B₄C-ZrB₂ composite (flat) against the cemented tungsten carbide ball is further discussed below:

From the observations it is clear that the COF is a function of load. The friction between two sliding bodies results in an increase of the contact temperature, which leads to deformation, cracking, and tribo-oxidative reactions [31]. The EDS pattern observed for all the wear scars revealed tungsten, carbon and oxygen. The source of tungsten was from the counter body material. Carbon may come from boron carbide as well as the counter body material. The presence of an oxygen peak indicates tribo-oxidation of the B₄C-ZrB₂ composite. The optical image of the wear scar formed on the WC ball (counter body) revealed the presence of a worn surface with deep abrasive grooves which points to the formation of tribo-oxidation layer on the counter body as well. The low COF and specific wear rate recorded in the present study may be caused by the formation of a tribo-oxide layer with lubricant property. The heat generated due to friction between the sliding surfaces is sufficient for the oxidation of B₄C (flat material) according to the reaction below to form B₂O₃ [28, 29, 31]. The oxygen required for the reaction can be supplied by the surrounding air. During cooling to room temperature, the B₂O₃ reacts with moisture in the air to form a secondary film, boric acid (H₃BO₃) as per reactions 5 to 7. Reaction 7 may also occur at localized tribo-contact regions.



In the present study, the volume of wear scar increased with increasing load and lead to an increase in the wear scar width and depth. This phenomenon may occur due to deformation at higher loads and delamination of tribo-oxide layers by cracking.

The wear rate for the composite varied in the order of 10⁻⁵ mm³·(N·m)⁻¹. The variation in the wear rate with changing load was due to providing more opportunity to form an oxide layer on the surface. Later this oxide layer acted as a solid lubricant in the form of a third body for the tribocouple [29]. It is found that the third body for-

mation plays a pivotal role to reduce friction and wear rate by absorbing the energy for deformation. However, at 20 N load, a slight increase in the wear rate was observed due to higher wear volume compared to the product of load and sliding distance. Increase in wear volume from 10 N to 20 N was observed due to the higher degree of microfracturing, as is strongly supported by SEM images (Figure 14). It can be summarized that the COF decreased from 0.24 to 0.15 when the load is increased from 5 N to 20 N. The specific wear rate observed was of the order of $10^{-5} \text{ mm}^3 \cdot (\text{N}\cdot\text{m})^{-1}$. At lower loads abrasive wear is dominant, while at higher loads tribo-oxidation is the dominant wear mechanism.

Addition of ZrO_2 to B_4C resulted in improved densification behavior. Reinforcement of ZrB_2 phase in B_4C yielded composite material with improved mechanical properties, thermo-physical properties and tribological properties as compared with monolithic boron carbide of similar density.

CONCLUSIONS

In the present study the microstructure, mechanical, thermophysical and wear properties of in-situ formed B_4C - ZrB_2 composite was investigated. The key findings can be summarized as follows:

- Formation of ZrB_2 as a reaction product was observed in the composite.
- The electrical resistivity value measured was $3.02 \times 10^{-4} \Omega\cdot\text{m}$ at 1000°C .
- The thermal conductivity measured from room temperature up to 1000°C was in the range of $8 - 10 \text{ W}\cdot\text{m}^{-1}\cdot\text{K}^{-1}$.
- The flexural strength dropped to 92 MPa from 176 MPa, when the samples are heated from room temperature to 900°C .
- The average value of coefficient of friction (COF) was measured as 0.15 at 20 N load and 10 Hz frequency. Increasing the load from 5 N to 20 N resulted in a decrease in COF by 37.5 % at 10 Hz frequency.
- Specific wear rate data observed was of the order of $10^{-5} \text{ mm}^3 \cdot (\text{N}\cdot\text{m})^{-1}$.
- Both abrasive and tribo-chemical reaction wear mechanisms were observed on the worn surface of the flat and the counter body materials.
- Dominant tribo-chemical reaction wear mechanism was observed at higher loads ($\geq 10 \text{ N}$).

Acknowledgement

The authors would like to acknowledge Sri C. Subramanian, Dr. A.K. Suri, Sri R.K. Fotedar, Dr. N. Krishnamurthy and Dr. R.C. Hubli for their valuable guidance and initiation of these activities. Also financial support by the Department of Atomic Energy (DAE), Government of India is gratefully acknowledged.

REFERENCES

1. Riedel R. (2000). Handbook of Ceramic Hard Materials, Vol. 2. Wiley-VCH Verlag GmbH.
2. Bauccio M.L. (1994). ASM Engineered Materials Reference Book, ASM International.
3. Suri A.K., Subramanian C., Sonberand J.K., Murthy T.S.R.Ch. (2010): Synthesis and consolidation of boron carbide: a review. *International Materials Review*, 55(1), 4-40. doi:10.1179/095066009X12506721665211
4. An Q., Goddard W.A. (2017): Nanotwins soften boron-rich boron carbide (B_{13}C_2). *Applied Physics Letters*, 110, 111902, 1-4. doi:10.1063/1.4978644
5. Watts J.L., Talbot P.C., Alarco J.A., Mackinnon I.D.R. (2017): Morphology control in high yield boron carbide. *Ceramics International*, 43, 2650–2657. doi:10.1016/j.ceramint.2016.11.076
6. Pillai H.G., Madam A.K., Chandra S., Cheruvalath V.M. (2017): Evolutionary algorithm based structure search and first-principles study of B_{12}C_3 polytypes. *Journal of Alloys and Compounds*, 695, 2023-2034. doi: 10.1016/j.jallcom.2016.11.040
7. Diaz-Cano A., Trice R.W., Youngblood J.P. (2017): Stabilization of highly-loaded boron carbide aqueous suspensions. *Ceramics International*, 43, 8572–8578. doi: 10.1016/j.ceramint.2017.03.111
8. Gunnewiek R.F.K., Souto P.M., Kiminami R.H.G.A. (2017): Synthesis of nanocrystalline boron carbide by direct microwave carbothermal reduction of boric acid. *Journal of Nanomaterials*, Article ID 3983468. doi:10.1155/2017/3983468
9. Ahmed Y.M.Z., El-Sheikh S.M., Ewais E.M.M., Abd-Allah A.A., Sayed S.A. (2017): Controlling the morphology and oxidation resistance of boron carbide synthesized via carbothermic reduction reaction. *Journal of Materials Engineering and Performance*, 26, 1444–1454. doi:10.1007/s11665-017-2548-3
10. Sedlák R., Kovařčíková A., Múdra E., Rutkowski P., Dubiel A., Girman V., Bystrický R., Dusza J. (2017): Boron carbide/graphene platelet ceramics with improved fracture toughness and electrical conductivity. *Journal of the European Ceramic Society*, (Article in Press). doi:10.1016/j.jeurceramsoc.2017.04.061
11. An Q. (2017): Prediction of superstrong τ -boron carbide phase from quantum mechanics. *Physical Review B*, 100101(R). doi:10.1103/PhysRevB.95.100101
12. Murthy T.S.R.Ch., Mukherjee A. (2006): Densification of boron carbide and titanium diboride. *Metals Materials And Processes*, 18(2), 151-158.
13. Subramanian C., Suri A.K., Murthy T.S.R.Ch. (2010): Development of boron – based materials for nuclear applications (technology development article). *BARC News Letter*, 313, 14-22. <http://barc.gov.in/publications/nl/2010/20100304.pdf>
14. Sonber J.K., Murthy T.S.R.Ch., Sairam K., Bedse R.D., Hubli R.C., Chakravarty J.K. (2015): Development and production of ^{10}B enriched boron carbide (B_4C) pellets for control rod application in PFBR (founder's day special issue). *BARC News Letter*, 259-264. <http://barc.gov.in/publications/nl/2015/spl2015/completeissue/complete-issue.html>
15. Sairam K., Sonber J.K., Murthy T.S.R.Ch., Paul B., Nachiket K., Jothilakshmi N., Bedse R.D., Kain V. (2016) Processing and properties of boron carbide with hafnium diboride addition. *Ceramics-Silikáty*, 60(4), 330-337. doi:10.13168/cs.2016.0049

16. Murthy T.S.R.Ch., Sonber J.K., Sairam K., Bedse R.D., Chakarvartty J.K. (2016): Development of refractory and rare earth metal borides and carbides for high temperature applications (ARRMA-2016). *Materials Today: Proceedings*, 3, 3104-3113. doi: 10.1016/j.matpr.2016.09.026
17. Sonber J.K., Murthy T.S.R.Ch., Subramanian C., Fotedar R.K., Hubli R.C., Suri A.K. (2013): Synthesis, densification and characterization of boron carbide. *Transactions of Indian Ceramic Society*, 72(2), 100-107. doi:10.1080/0371750X.2013.817755
18. Sairam K., Sonber J.K., Murthy T.S.R.Ch., Subramanian C., Fotedar R.K., Nanekar P., Hubli R.C. (2014): Influence of spark plasma sintering parameters on densification and mechanical properties of boron carbide. *International Journal of Refractory Metals and Hard Materials*, 42, 185-192. doi:10.1016/j.ijrmhm.2013.09.004
19. Sairam K., Sonber J.K., Murthy T.S.R.Ch., Subramanian C., Hubli R.C., Suri A.K. (2012): Development of B₄C-HfB₂ composites by reaction hot pressing. *International Journal of Refractory Metals and Hard Materials*, 35, 32-40. doi:10.1016/j.ijrmhm.2012.03.004
20. Kumar S., Sairam K., Sonber J.K., Murthy T.S.R.Ch., Reddy V., Rao G.V.S. N., Rao T.S. (2014): Hot-pressing of MoSi₂ reinforced B₄C composites. *Ceramics International*, 40, 16099-16105. doi:10.1016/j.ceramint.2014.06.135
21. Moskovskikh D.O., Paramonov K.A., Nepapushev A.A., Shkodich N.F., Mukasyan A.S. (2017): Bulk boron carbide nanostructured ceramics by reactive spark plasma sintering. *Ceramics International*, 43, 8190-8194. doi:10.1016/j.ceramint.2017.03.145
22. Subramanian C., Roy T.K., Murthy T.S.R.Ch., Sengupta P., Kale G.B., Krishnaiah M.V., Suri A.K. (2008): Effect of zirconia addition on pressureless sintering of boron carbide. *Ceramics International*, 34, 1543-1549. doi:10.1016/j.ceramint.2007.04.017
23. Goldstein A., Yeshurun Y., Goldenberg A. (2007): B₄C/metal boride composites derived from B₄C/metal oxide mixtures. *Journal of the European Ceramic Society*, 27 (2-3), 695-700. doi:10.1016/j.jeurceramsoc.2006.04.042
24. Yue X.Y., Zhao S.M., Lu P., Chang Q., Ru H.Q. (2010): Synthesis and properties of hot pressed B₄C-TiB₂ ceramic composite. *Materials Science and Engineering: A*, 527, 7215-7219. doi:10.1016/j.msea.2010.07.101
25. Sonber J.K., Limaye P.K., Murthy T.S.R.Ch., Sairam K., Nagaraj A., Soni N.L., Patel R.J., Chakarvartty J.K. (2015): Tribological properties of boron carbide in sliding against WC ball. *International Journal of Refractory Metals and Hard Materials*, 51, 110-117. doi:10.1016/j.ijrmhm.2015.03.010
26. Li X., Gao Y., Wei S., Yang Q. (2017): Tribological behaviors of B₄C-hBN ceramic composites used as pins or discs coupled with B₄C ceramic under dry sliding condition. *Ceramics International*, 43, 1578-1583. doi:10.1016/j.ceramint.2016.10.136
27. Sahani P., Chaira D. (2017): Nonlubricated sliding wear behavior study of SiC-B₄C-Si cermet against a diamond indenter. *Journal of Tribology*, 139, 051601, 1-13. doi:10.1115/1.4035344
28. Larsson P., Axen N., Hogmark S. (1999): Tribofilm formation on boron carbide in sliding wear. *Wear*, 236, 73-80. doi:10.1016/S0043-1648(99)00266-5
29. Erdemir A., Bindal C., Zuiker C., Savrun E. (1996): Tribology of naturally occurring boric acid Films on boron carbide. *Surface and Coatings Technology*, 86-87, 507-510.
30. Poliarus O., Umanskyi O., Ukrainets M., Kostenko O., Antonov M., Hussainova I. (2016): Influence of Cr, Ti and Zr oxides formation on high temperature sliding of NiAl-based plasma spray coatings. *Key Engineering Materials*, 674, 308-312. doi:10.4028/www.scientific.net/KEM.674.308
31. Quinn T.F.J. (1992). Oxidational wear. in: ASM Handbook, Vol 19. 9th ed. pp. 289-290.
32. Murthy T.S.R.Ch., Limaye P.K., Sonber J.K., Sairam K., Nagaraj A., Subramanian C., Soni N.L., Patel R.J., Hubli R.C. (2014): Friction and wear properties of hot pressed (Ti,Cr)B₂-MoSi₂ composite in sliding against WC ball. *International Journal of Refractory Metals and Hard Materials*, 43, 276-283. doi:10.1016/j.ijrmhm.2013.12.013
33. Bhatt B., Murthy T.S.R.Ch., Limaye P.K., Nagaraj A., Singh K., Sonber J.K., Sairam K., Sashanka A., Rao G.V.S.N., Rao T.S. (2016): Tribological studies of monolithic chromium diboride against cemented tungsten carbide (WC-Co) under dry condition. *Ceramics International*, 42, 15536-15546. doi:10.1016/j.ceramint.2016.06.208
34. Murthy T.S.R.Ch., Basu B., Shrivastava A., Balasubramanian R., Suri A.K. (2006): Tribological properties of TiB₂ and TiB₂-MoSi₂ ceramic composites. *Journal of the European Ceramic Society*, 26, 1293-1300. doi:10.1016/j.jeurceramsoc.2005.01.054
35. Raju G.B., Basu B. (2009): Influence of MoSi₂ addition on load dependent fretting wear properties of TiB₂ against cemented carbide. *Journal of the American Ceramic Society*, 92(9), 2059-2066. doi:10.1111/j.1551-2916.2009.03173.x
36. Amartya M., Raju G.B., Basu B. (2008): Understanding influence of MoSi₂ addition (5 weight percent) on tribological properties of TiB₂. *Metallurgical and Materials Transactions: A*, 39(12), 2998-3013. doi:10.1007/s11661-008-9652-9
37. Bhatt B., Murthy T.S.R.Ch., Nagaraj A., Singh K., Sonber J.K., Sairam K., Sashanka A., Rao G.V.S.N., Rao T.S., Kain V. (2017): Wear behaviour of CrB₂-5 wt.% MoSi₂ composite against cemented tungsten carbide (WC-Co) under dry reciprocative sliding condition. *Journal of the Australian Ceramic Society*, 53(2), 611-625. doi:10.1007/s41779-017-0073-3
38. Sonber J.K., Murthy T.S.R.Ch., Sairam K., Nagaraj A., Singh K., Bedse R.D., Majumdar S., Kain V. (2017): Development and tribological properties of SiC fibre reinforced CrB₂ composite. *Journal of the Australian Ceramic Society*, 53(2), 309-317. doi:10.1007/s41779-017-0039-5
39. Antis G.R., Chantikul P., Lawn B.R., Marshall D.B. (1981): A critical evaluation of indentation techniques for measuring fracture toughness: I, direct crack measurements. *Journal of the American Ceramic Society*, 64, 533-538. doi:10.1.1.204.2314
40. Standard test method for linearly reciprocating ball-on-flat sliding wear Annual Book of ASTM Standards, vol. 03.02, ASTM G 133-05, 2005.
41. Pabst W., Gregorová E. (2014): Conductivity of porous materials with spheroidal pores. *Journal of the European Ceramic Society*, 34(11), 2757-2766. doi:10.1016/j.jeurceramsoc.2013.12.040
42. Fromet K., Chatillon C., Fouletier J., Fouletier M. (1992): Carbon activity measurements in boron carbides using a solid state potentiometric cell. *Journal of Nuclear Materials*, 188, 280-284. doi:10.1016/0022-3115(92)90485-4
43. Gosset D., Colin M., (1991): Boron carbides of various compositions: an improved method for X-rays characterization. *Journal of Nuclear Materials*, 183, 161-173.